DOI: 10.1002/chem.200500981

π Topology and Spin Alignment in Unique Photoexcited Triplet and Quintet States Arising from Four Unpaired Electrons of an Organic Spin System

Yoshio Teki,* Tetuya Toichi, and Satoru Nakajima[a]

Abstract: Syntheses, electronic structures in the ground state, unique photoexcited states, and spin alignment are reported for novel biradical **1**, which was designed as an ideal model compound to investigate photoinduced spin alignment in the excited state. Electron spin resonance (ESR), time-resolved ESR (TRESR), and laser-excitation pulsed ESR experiments were carried out. The magnetic properties were examined with a SQUID magnetometer. In the electronic ground state, two radical moieties interact very weakly (almost no interaction) with each other through the closed-shell diphenylanthracene spin coupler. On photoirradiation, a novel lowest photoexcited state with the intermediate spin ($S=1$) arising from four unpaired electrons with low-lying quintet ($S=2$) photoexcited state was detected. The unique triplet state has an interesting electronic structure, the D value of which is reduced by antiferromagnetic spin alignment between two radical spins through the excited triplet spin coupler. The general theoretical predictions of the spin alignment and the reduction of the fine-structure splitting of the triplet bis(radical) systems are presented. The fine-structure splitting of the unique photoexcited triplet state of **1**, as well as the existence of the low-lying quintet state, is interpreted well on the basis of theoretical predictions. Details of the spin alignment in the photoexcited states are discussed.

Keywords: EPR spectroscopy · magnetic properties · pi topology · radicals · spin alignment

Introduction

π-Conjugated spin systems constructed from aromatic hydrocarbons and dangling stable radicals are ideal model systems to study the relationship between π topology and spin alignment in the photoexcited states. Hereafter, we call these molecules "π-conjugated photoexcited spin systems". The delocalized π orbital network is most important in determining the spin states in the photoexcited states[1–3] and ground states.[4–6] Spin manipulation is a challenging topic in the field of molecular magnetism.[7,8]

We earlier reported spin manipulation using the photoexcited molecular field in purely organic π-conjugated spin systems, in which parallel alignment of two pendant radical spins through an excited triplet spin coupler leads to the photoexcited quintet ($S=2$) high-spin state.[1–3,9] The nature of the exchange coupling between two pendant radical spins through the spin coupler changes from antiferromagnetic to ferromagnetic on photoexcitation. We have also reported other π-conjugated photoexcited high-spin systems,[10–12] which were designed by using π topology. Spin manipulation of the π-conjugated organic spin systems in the ground state have been also intensively investigated by using electron hole doping[13] and photochromic molecules.[14]

The π topology plays a key role in spin manipulation and molecular design of π-conjugated organic high-spin systems. π-Conjugated photoexcited spin systems have the following advantages compared to other triplet-radical pair systems (σ-bonded systems[15] and metal coordination complexes[16]) from the viewpoint of the materials science and molecular magnetism: 1) π Conjugation leads to strong exchange coupling, which is one of the important conditions for the appearance of bulk magnetism at finite temperature. 2) One can design and synthesize appropriate spin systems with desired spin states using well-established synthetic chemistry. 3) An enhanced intersystem crossing (ISC) mechanism arising from the attachment of the radical species is available.[2] This opens the way to direct ESR detection of the aromatic hydrocarbons, which have ESR-silent photoexcited states as the result of the low efficiency of ISC to their triplet states.

[a] Prof. Y. Teki, T. Toichi, S. Nakajima
Department of Material Science
Graduate School of Science, Osaka City University
3-3-138 Sugimoto, Sumiyoshi-ku, Osaka 558-8585 (Japan)
Fax: (+81) 6-6605-2559
E-mail: teki@sci.osaka-cu.ac.jp

Supporting information for this article is available on the WWW under http://www.chemeurj.org/ or from the author.

Chemically induced dynamic electron polarization between the radical and the excited triplet state has been extensively investigated in solution.[17] However, such enhanced ISC effects were not reported for their intermolecular triplet-radical pairs. This type of enhanced ISC is expected to occur only in π-conjugated spin systems.

Compound **1** shown in Figure 1 was designed and synthesized by considering the above-mentioned advantages, and is an important model compound for investigating spin alignment in photoexcited states for the following two reasons: 1) Both ferromagnetic and antiferromagnetic coupling between the pendant radical spins and the photoexcited triplet moiety are expected to coexist in **1**. 2) As a result of spin-exchange coupling through the photoexcited spin coupler, it is expected to have unique photoexcited spin states; the lowest triplet state arises from four unpaired electrons with a nearly degenerate quintet state, as shown below. For spin systems with four unpaired electrons, spin states with $S=2$, 1, and 0 exist, and normally either the low-spin ($S=0$) or the high-spin ($S=2$) state is the lowest photoexcited state. However, one can design a molecule with intermediate spin ($S=1$) as the lowest photoexcited state by taking π topology into account. According to our previous work,[2,3] *meta*-joint configuration between the iminonitroxide radical and the triplet excited state of the anthracene moiety leads to antiferromagnetic coupling, and *para*-joint configuration to ferromagnetic coupling. Therefore, as illustrated in Figure 1, **1** will have the state with intermediate spin ($S=1$) as the lowest photoexcited state. The photoexcited triplet state has an interesting electronic structure with respect to spin correlation.

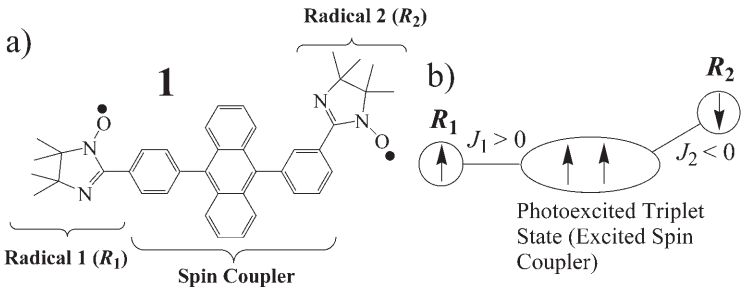

Figure 1. Molecular structure of **1** and schematic picture of the expected spin alignment in the lowest photoexcited state.

Previously,[12] we reported briefly on the photoexcited triplet and quintet states of **1**. Here we describe in detail spin alignment in both the ground state and photoexcited states of **1**. The general theoretical predictions of the spin alignment and the reduction of the fine-structure splitting of the triplet–bis(radical) system are presented. The fine-structure splitting of the unique triplet photoexcited state of **1** and the existence of the low-lying quintet state are interpreted on the basis of theoretical predictions. Synthesis, electronic state, magnetic properties in the ground state, the photoexcited states, and their spin alignment are reported. Continuous-wave (CW) ESR, time-resolved ESR (TRESR), and laser-excitation pulsed ESR experiments were carried out. The magnetic properties were examined with a SQUID magnetometer.

Theoretical Predictions

To clarify photoinduced spin alignment due to the photoexcited triplet spin coupler, a theoretical study based on the spin Hamiltonian was carried out. Here we report the general theoretical prediction of the energy ordering and the relationship of the fine-structure parameters of each spin state of the triplet–bis(radical) system illustrated in Figure 2,

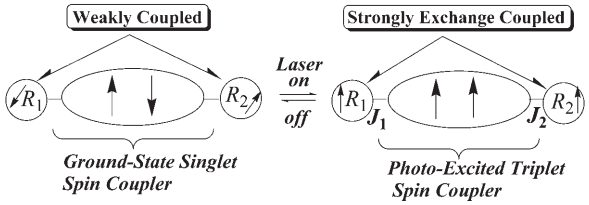

Figure 2. Schematic pictures of photoinduced spin alignment through the spin coupler.

which is constructed from four electron spins. We treat the whole spin Hamiltonian for the triplet-bis(radical) system. In **1**, the diphenylanthracene moiety plays the role of spin coupler, which is the spin-paired singlet in the ground state and becomes the photoexcited triplet state on the photoexcitation. Two pendant radicals interact with each other through the singlet (ground state) or triplet (photoexcited state) spin coupler. The total spin Hamiltonian of the four-spin system [photoexcited triplet–bis(radical)] is given by Equations (1) and (2).

$$H_{\mathrm{spin}} = H_{\mathrm{ex}} + \beta_e H \cdot \boldsymbol{g}^{\mathrm{T}} \cdot \boldsymbol{S}^{\mathrm{T}} + \beta_e H \cdot \boldsymbol{g}^{\mathrm{R1}} \cdot \boldsymbol{S}^{\mathrm{R1}} + \beta_e H \cdot \boldsymbol{g}^{\mathrm{R2}} \cdot \boldsymbol{S}^{\mathrm{R2}} + \boldsymbol{S}^{\mathrm{T}} \cdot \boldsymbol{D}(\mathrm{T}) \cdot \boldsymbol{S}^{\mathrm{T}} + \boldsymbol{S}^{\mathrm{R1}} \cdot \boldsymbol{D}(\mathrm{R_1T}) \cdot \boldsymbol{S}^{\mathrm{T}} + \boldsymbol{S}^{\mathrm{R2}} \cdot \boldsymbol{D}(\mathrm{R_2T}) \cdot \boldsymbol{S}^{\mathrm{T}} \quad (1)$$

$$H_{\mathrm{ex}} = -2J_1 \boldsymbol{S}^{\mathrm{R1}} \cdot \boldsymbol{S}^{\mathrm{T}} - 2J_2 \boldsymbol{S}^{\mathrm{T}} \cdot \boldsymbol{S}^{\mathrm{R2}} \quad (2)$$

Here we omit the dipolar interactions between the two radical moieties. In π-conjugated spin systems, the exchange interaction is much larger than the other interactions in Equation (1). The energies of each spin state in zero magnetic field were therefore obtained to zeroth order by diagonalizing H_{ex}. The expectation values of the fine-structure terms of each spin state were calculated by using the eigen-

functions. In this calculation, we also omitted $D(R_1T)$ and $D(R_2T)$ in Equation (1), because $D(T)$ is much larger than them. There are two kinds of triplet states (T_1 and T_2), one quintet state (Qu), and one singlet state (S). The energy versus J_2/J_1 diagrams for the spin states are shown in Figure 3a. The fine-structure terms D of each spin state are related to the fine-structure tensor $D(T)$ of the triplet state of anthracene by a reduction factor f [$D = f \cdot ED(T)$]. The J_2/J_1 dependences of the reduction factor f of the fine-structure tensor for the spin states are shown in Figure 3b.

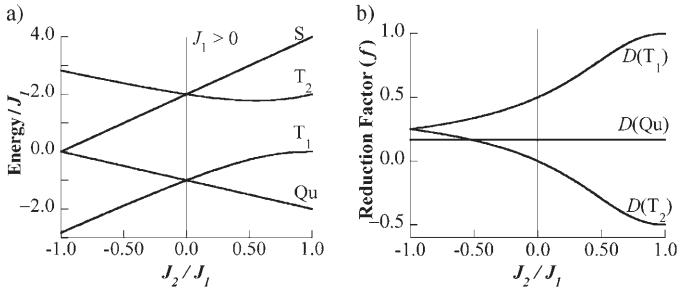

Figure 3. J_2/J_1 dependence of the energy levels of the photoexcited states and their reduction factors f of each spin state.

The analytical expressions of the energy and the reduction factors of each spin state are given by Equations (3a)–(3d)

$$E_{Qu} = -(1+\alpha)J_1 \quad f_{Qu} = 1/6 \tag{3a}$$

$$E_{T1} = \lambda_- J_1 \quad f_{T1} = \frac{a_1^2 + b_1^2 - 2}{a_1^2 + b_1^2 + 1} \tag{3b}$$

$$E_{T12} = \lambda_+ J_1 \quad f_{T12} = \frac{a_2^2 + b_2^2 - 2}{a_2^2 + b_2^2 + 1} \tag{3c}$$

$$E_s = (2+2\alpha)J_1, f_s = 0 \tag{3d}$$

where [Eqs. (4a)–(4d)]

$$\alpha = J_2/J_1 \tag{4a}$$

$$\lambda_\pm = \frac{1+\alpha \pm \sqrt{(1+\alpha)^2 + 8(1-\alpha)^2}}{2} \tag{4b}$$

$$a_1 = \frac{\sqrt{2}\alpha}{-1+\alpha-\lambda_-} \quad b_1 = \frac{\sqrt{2}}{1-\alpha-\lambda_-} \tag{4c}$$

$$a_2 = \frac{\sqrt{2}\alpha}{-1+\alpha-\lambda_+} \quad b_2 = \frac{\sqrt{2}}{1-\alpha-\lambda_+} \tag{4d}$$

These analytical solutions were tested by the exact numerical diagonalization of Equation (1).

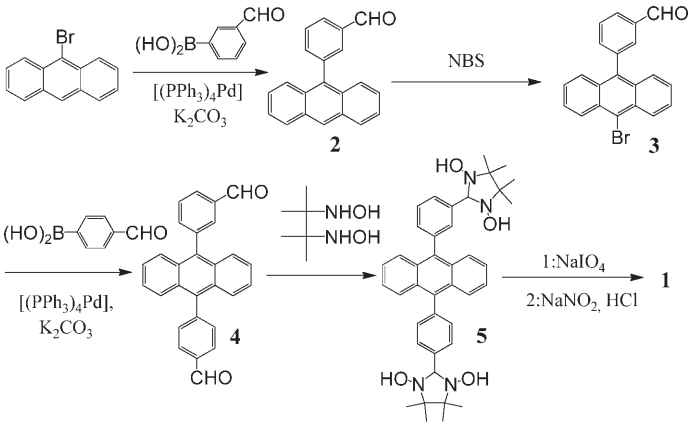

Scheme 1. Synthesis of **1**.

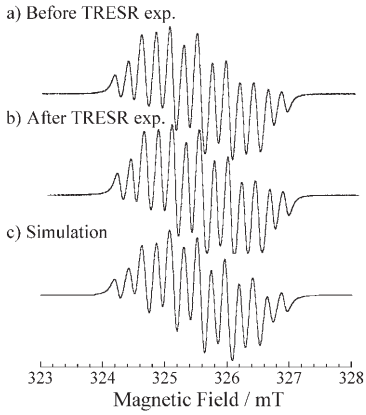

Figure 4. Solution ESR spectra of **1** at room temperature. Isopentane/diethyl ether (2/3) was used to carry out the TRESR experiments in the glass matrix. a) Before TRESR measurement. b) After TRESR measurement. c) Spectrum simulated by using the g and HFCC vales listed in Table 1.

Results and Discussion

Ground state of 1: Compound **1** was synthesized according to Scheme 1. Figure 4 shows the solution ESR spectra at room temperature observed before and after TRESR experiments and the spectral simulation. Isopentane/diethyl ether (2/3) was used for all of the ESR experiments. This mixed solvent becomes a clear rigid glass matrix at low temperature. The solution ESR spectrum of **1** was well analyzed by a spectral simulation. The g value and the hyperfine coupling constants (HFCC) of the four nitrogen atoms are listed in Table 1 together with those of the *para*- and *meta*-jointed phenylanthracene(iminonitroxide) mono-radicals (*para*- and *meta*-AIN). The HFCCs of **1** are about one-half of those of the monoradicals, which is a characteristic feature of biradicals. The two radical moieties of **1** are coupled weakly to each other through the closed-shell diphenylanthracene spin coupler. One set of HFCCs ($A_{N(1)}$ and $A_{N(2)}$) of **1** are close to one-half of those of *para*-AIN, and another set of HFCCs ($A_{N(3)}$ and $A_{N(4)}$) is also close to one-half of those of *meta*-AIN, that is, the two iminonitroxide units are

Table 1. *g* values and hyperfine coupling constants of **1** and *para*- and *meta*-phenylanthracene(iminonitroxide) monoradicals (AIN) in their electronic ground states.

	g	Hyperfine coupling constants [mT]
1	2.0061	$A_{N(1)}=0.465$, $A_{N(2)}=0.210$, $A_{N(3)}=0.414$, $A_{N(4)}=0.250$
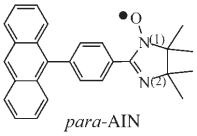 *para*-AIN	2.0063	$A_{N(1)}=0.900$, $A_{N(2)}=0.420$
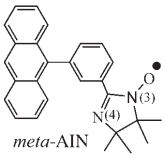 *meta*-AIN	2.0062	$A_{N(3)}=0.850$, $A_{N(4)}=0.450$

attached at nonsymmetric positions (*para* and *meta* positions). The same ESR pattern was observed before and after prolonged TRESR experiments, that is, **1** is quite stable to laser excitation ($\lambda=355$ nm) in the rigid glass matrix.

The temperature dependence of the magnetic susceptibility was examined with a SQUID magnetometer. Figure 5

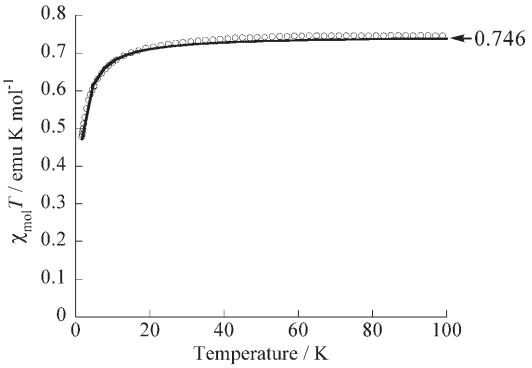

Figure 5. χT versus T plot of a powder sample of **1**. The decrease in the χT value in the low-temperature region is due to intermolecular (not intramolecular) magnetic interaction.

shows the $\chi_{mol}T$ versus T plot of the molar magnetic susceptibility χ_{mol} of a powder sample. The purity of the sample was tested by means of the magnetic susceptibility data. The $\chi_{mol}T$ value at 300 K of 0.746 emu K mol^{-1} showed that the purity of the sample was higher than 99%, because 0.375 corresponds to the magnetic moment of $S=1/2$ per mole. The decrease of the $\chi_{mol}T$ value in the low-temperature region is due to intermolecular (not intramolecular) magnetic interaction. The temperature dependence was well analyzed by using the Curie–Weiss law with intermolecular antiferromagnetic interaction of $\theta=-1.0$ K. The temperature dependence of the ESR signal intensity of **1** diluted in the glass matrix obeyed the simple Curie law $I_{ESR}\sim$const./T, that is, spin coupling between the two dangling radicals through the diphenylanthracene spin coupler (spin singlet) in the ground state is very weak. This is reasonable because the *meta*-joint configuration is at the disjoint position in the Borden–Davidson definition.[18]

Results of TRESR experiments: To study the photoexcited state, TRESR experiments were performed at 30 K in the glass matrix. Significant temperature dependence of the spectrum was not observed from 10 to 40 K. Details of our TRESR setup were described previously.[2] Figure 6a shows a typical TRESR spectrum of **1** observed 0.5 μs after laser excitation ($\lambda=355$ nm), and Figure 6b is the spectral simula-

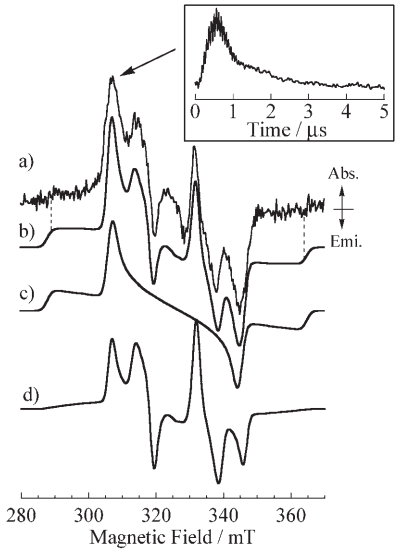

Figure 6. TRESR spectrum of **1** and the spectral simulations. a) Observed spectrum 0.5 μs after the laser excitation. b) Simulated spectrum (superimposition of the triplet (c) and the quintet (d) spectra). c) Simulation of the triplet-state spectrum. d) Simulation of the quintet state spectrum.

tion, carried out with the eigenfield[19]/exact-diagonalization hybrid method.[20] The TRESR spectrum was very well simulated by a superimposition with equal weight of a triplet (T_1) and quintet (Qu) spectrum. The decay profile shows the existence of two components with different lifetimes or spin relaxation times (inset of Figure 6), and this supports the superimposition of triplet and quintet signals shown by the simulation. The spin Hamiltonian parameters of the triplet state ($S=1$), determined by spectral simulation, are listed in Table 2. These values are in agreement with those determined by pulsed-ESR experiments (see below). The simulated spectrum of the triplet state is shown in Figure 6c. The spin Hamiltonian parameters of the quintet ($S=2$) state (Table 2) were determined from the spectral simulation shown in Figure 6d. These simulated spectra were obtained under the assumption that the lowest energy M_S sublevels of both spin states were selectively populated in zero magnetic field. Thus, the relative populations (electron spin polarization, ESP) of each M_S sublevel in T_1 and Qu have been determined to be $P_{0'}=1.0$ and $P_{1'}=P_{-1'}=0.0$ for T_1 and $P_{0'}=$

Table 2. *g* values and zero-field splitting parameters and relative populations (polarization) for each zero-field spin sublevel of the triplet (T1) and the quintet (Qu) excited states of **1**. $P_{M_S'}$ means the population of spin sublevel in zero magnetic field, which is correlated to the $|S, M_S\rangle$ sublevel in the high-field limit.

	g	*D* [cm^{-1}]	*E* [cm^{-1}]	Relative populations
T_1	2.0045	0.0360	0.0	$P_{0'}:P_{+1'}:P_{-1'}=1.0:0.0:0.0$ (TRESR)
		0.0355	0.0	$P_{0'}:P_{+1'}:P_{-1'}=1.0:0.0:0.0$ (pulsed ESR)
Qu	2.0050	0.0125	0.0	$P_{0'}:P_{+1'}:P_{-1'}:P_{-2'}:P_{+2'}=1.0:0.0:0.0:0.0:0.0$ (at 0.5 μs)
				$P_{0'}:P_{+1'}:P_{-1'}:P_{-2'}:P_{+2'}=0.30:0.35:0.35:0.0:0.0$ (at 2.0 μs)

1.0, $P_{-1'}=P_{1'}=0.0$, and $P_{-2'}=P_{+2'}=0.0$ for Qu (Table 2) with increasing order of energy in zero magnetic field from the spectral simulation. Here, $P_{M_S'}$ means the population of the spin sublevel in zero magnetic field, which is correlated to the $|S, M_S\rangle$ sublevel in the high-field limit. Interestingly, this initial electron spin polarization of the quintet state observed at 0.5 μs differs from that of the *para*-joint π-topological isomer *p*,*p*-diphenylanthracene-bis(iminonitroxide) biradical, for which the lowest quintet state was reported previously.[2,9] The spectral pattern changed with time. Figure 7 shows the spectrum at 2.0 μs, which was simulated by the pure quintet state with ESP close to the lowest photoexcited quintet state of the π-topological isomer reported previously.[1,2] Thus, the relative population of the photoexcited quintet state of **1** changes dynamically from ($P_0=1.0$, $P_{\pm1'}=P_{\pm2'}=0.0$) to ($P_{0'}=0.30$, $P_{\pm1'}=0.35$, $P_{\pm2'}=0.0$). Such time dependence of ESP was not observed for the lowest photoexcited quintet states of the *para*-joint π-topological isomer[2] and the *para*-joint verdazyl biradical[9] This phenomenon may come from the situation that the quintet state is the low-lying photoexcited state closely located above the triplet state (see below).

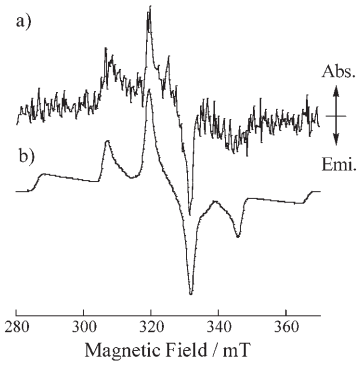

Figure 7. TRESR signal observed at the time of the triplet signal to be relatively decreased. a) Observed spectrum 2.0 μs after laser excitation. b) Simulated spectrum for the pure quintet state with the same spin Hamiltonian parameters as in the text. The relative populations of the M_S sublevels are $P_{0'}=0.30$, $P_{\pm1'}=0.35$, $P_{\pm2'}=0.0$ (Table 2). The relative populations are different from the initial ones.

Results of pulsed-ESR experiments: Figure 8a depicts the echo-detected ESR signal observed 0.5 μs after pulsed-laser excitation. The strong signal at the center of the spectrum is due to the ground state, and other signals come from the photoexcited state, which was confirmed by comparison with the spectrum without photoexcitation. As shown in Figure 8b, the observed spectrum assigned to the photoexcited state was well simulated predominantly as a triplet state ($S=1$) with the spin Hamiltonian parameters listed in Table 2. The magnitude of the fine-structure parameters was in good agreement with the values determined by spectral simulation of the TRESR spectrum (see above). The *D* value of the triplet state was accurately determined in this pulsed-ESR experiment. To confirm the spin state, transient nutation spectroscopy[21] was carried out. The transient nutation behaviors of the signals at 298.4 (upper) and at 317.0 mT (lower) are shown in Figure 8c. The periods of the echo signal intensity for the microwave pulse length were 194.4 and 289.8 ns, respectively. The ratio of the nutation frequency was determined to be 1.49 from the periods.[28] The nutation frequency ω of the $M_S \leftrightarrow M_S+1$ transition is given under the condition of each M_S transition being well distinguishable ($\omega_1 \ll \omega_{ZFS}$) by Equation (5), where $\omega_1 = g\beta_e B_1/\hbar$, $\omega_{ZFS}=D/\hbar$, and B_1 is the field strength (strictly speaking, the magnetic field flux density) of the microwaves.[21] Therefore, in the triplet state, the expected nutation frequency is $\sqrt{2}\omega_1$, because $S=1$ and $M_S=0$ or -1 (the ±1 to 0 ESR transitions).

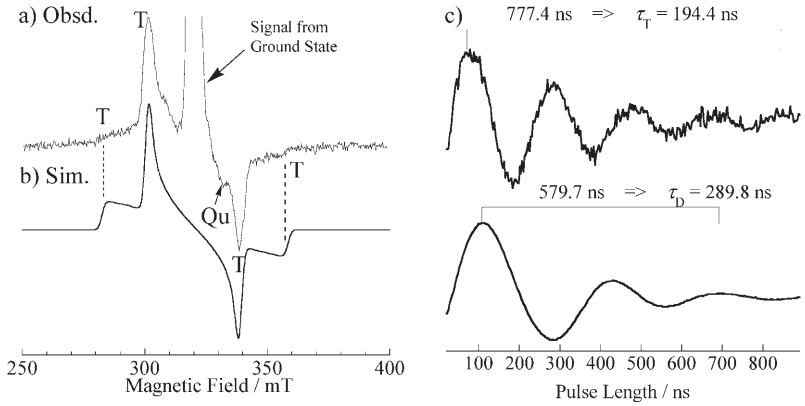

Figure 8. Echo-detected pulsed ESR spectrum of **1**. a) Observed spectrum 0.5 μs after laser excitation. T and Qu denote the signals from the triplet and quintet states, respectively. b) Simulated spectrum of the triplet state. c) Transient nutation phenomena of the signals at 298.4 mT (top) and at 317.0 mT (bottom).

$$\omega = \sqrt{S(S+1)-M_S(M_S+1)}\,\omega_1 \qquad (5)$$

The observed value (1.49) is close to $\sqrt{2}$,[28] which is the theoretical value expected for the ratio of the nutation frequencies between the triplet and doublet states. The ground state of **1** is a very weakly coupled biradical. The ESR signal of the ground state of **1** in the glass matrix was a nearly symmetric single peak without fine-structure splitting. Thus, the M_S difference of the transitions was not distinguishable. In such a case, the nutation frequency should be the same as that of the doublet state (ω_1). It is well known that the nutation frequency becomes that of the doublet state under the condition $\omega_1 \gg \omega_{ZFS}$, which is satisfied in the ground state of **1** because the fine-structure splitting is included in the linewidth.[21,22] Actually, the nutation frequency of the ground state of **1** was close to that of the doublet ground state of the phenylanthracene monoradical. Therefore, the transient nutation experiments show that the signal observed at 298.4 mT can be assigned to the triplet state.[28] This finding supports the result of the spectral simulation of the echo-detected ESR signal. A two-dimensional (2D) nutation experiment[21b,22,15b] was impractical because of the long measuring time required for the accumulation resulting from the weak echo intensity. Figure 8a shows that the quintet state was not clearly observed with the pulse length that corresponds to making the signal intensity of the $M_S = 0 \leftrightarrow \pm 1$ transitions of the triplet state a maximum ($\pi/2$–τ–π pulse sequence for the transitions). When we chose the pulse length corresponding to the $\pi/2$–τ–π pulse sequence of the quintet state, the $M_S = 0 \leftrightarrow \pm 1$ transitions of the quintet state were weakly detected by intensive accumulation (see Figure S1, Supporting Information). The weak signals of the $M_S = 0 \leftrightarrow \pm 1$ transitions of the quintet state overlapped with the shoulders of the signals of the triplet state. Therefore, we can safely conclude that the photoexcited triplet state of **1** was selectively observed by echo-detected ESR by choosing the proper pulse length. The spin Hamiltonian parameters were more accurately determined by selective detection.

The detection of the FID signals did not succeed as a result of the dead time of the pulsed-ESR detection. The selective detection of the triplet state by using spin-echo detection of the ESR signal is the result of the shorter phase memory time T_M of the quintet state than of the triplet state, although the origin is not clear. To confirm this speculation, we measured T_M of the $M_S = 0 \leftrightarrow -1$ transitions of the triplet and quintet states from the $\pi/2$–π pulse interval dependence of the echo intensity (see Figure S2 in the Supporting Information). The T_M values of the triplet and quintet states were determined to be 697 and 299 ns, respectively. The T_M of the quintet state is about two times shorter than that of the triplet state. The short phase memory time may be related to the situation that the quintet state is the low-lying excited state located closely above the lowest photoexcited triplet state.

Spin alignment and fine-structure splitting in the photo-excited states: The magnitude of D of the triplet state detected in TRESR and pulsed-ESR is about 50% of that of anthracene.[23] This small D value is reasonably understood by the prediction shown in Figure 3b. According to the spin coupling shown in Figure 1b, **1** is expected to have the lowest photoexcited triplet state. The sign and magnitude of the exchange coupling between the radical moiety and the triplet spin coupler is proportional to the product of the spin densities at linking positions. The spin coupling at *meta*-joint configuration between the radical moiety and the triplet excited state of the anthracene moiety is expected to be antiferromagnetic, and the *para*-joint configuration leads to ferromagnetic coupling. Therefore, as shown in Figure 1b, J_1 and J_2 have positive and negative sign of the exchange interactions, respectively. The spin density at the linking carbon atom of the diphenylanthracene spin coupler for R_2 is expected to be small.[24] Therefore, a small negative value of J_2/J_1 is expected. According to Figure 3b, the reduction factor f becomes close to and smaller than 0.5 for the small negative value of J_2/J_1.

The reduction factor was estimated to be $f = 0.47$ from the ratio $D(T_1)/D(Qu)$, determined in the experiment. In this calculation, we adopted the $D(T_1)$ value determined from the pulsed-ESR experiment. This f value corresponds to $J_2/J_1 = -0.08$ in Figure 3b. This sign and magnitude are in agreement with those expected from the unique electronic structure of the photoexcited states of **1**. This result indicates strongly that **1** has a lowest photoexcited triplet state with low-lying quintet state. The quintet state is located very closely above the triplet state in this case. The observation of the quintet state in **1** is well understood from this situation.

This is the first direct detection of a lowest photoexcited triplet state with the reduced D value,[25] which comes from the unique electronic structure as the result of the antiferromagnetic spin alignment between the radical spins through the excited triplet spin coupler. This unique photoexcited triplet state will provide an ideal target to test molecular orbital theory for excited states.

Conclusion

We conclude that **1** has a unique lowest photoexcited triplet state arising from four unpaired electrons with a low-lying quintet photoexcited state closely above the triplet state. The unique triplet state has reduced fine-structure splitting. The reduced D value was well understood theoretically by the spin Hamiltonian approach for the triplet–bis(radical) four-spin system. The low-lying quintet excited state also has interesting characteristics; its initial electron polarization is different from that of the lowest photoexcited quintet state reported previously. These unique electronic structures and spin states are realized by antiferromagnetic spin exchange coupling between two radical spins through the photoexcited triplet spin coupler.

Experimental Section

Measurements: A conventional X-band ESR spectrometer (JEOL TE300) was used without field modulation in the TRESR measurements. TRESR signals were amplified by a wide-band preamplifier, transferred to a high-speed digital oscilloscope (LeCroy 9350C), and accumulated, typically 1400 times for each point. Excitation of **1** was carried out with 355 nm light from a YAG laser (Continuum Surelite II-10). The typical laser power used in the experiments was ca. 3–5 mJ. The temperature was controlled using an Oxford ESR 910 cold He gas flow system. All TRESR and pulsed ESR experiments were carried in isopentane/diethyl ether (2/3). Solvents of the highest commercially available purity were purified by the usual procedures. Samples were degassed by repeated freeze–pump–thaw cycles on a high-vacuum line system.

The echo-detected pulsed ESR measurements were performed on the X-band TE-300 spectrometer equipped with a pulsed microwave unit (JEOL ES-PX1150), an arbitrary wave pattern generator (Tektronix AWG500), a pulse buffer (JEOL PD1001), and a high-speed digital oscilloscope (Tektronix TDS5034). The pulsed microwaves were amplified with a 10 W solid-state amplifier (Microwave Power Inc., Model L0809–40). Hahn's $\pi/2$–τ–π pulse sequence was used for spin echo detection. The microwave pulse was synchronized with the laser excitation using a delay pulse generator (Stanford Research DG535). The excitation was also carried out with 355 nm light from the YAG laser. In the echo-detected nutation experiment, the pulse length of the first microwave pulse was changed, and the second pulse was set to π pulse, as schematically shown in Figure 9.

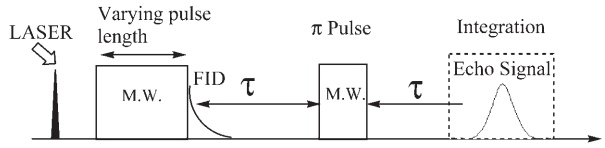

Figure 9. Schematic diagram of the echo-detected nutation experiment. In the excited-state measurements, laser excitation was used. The microwave pulse sequence was synchronized with the laser excitation.

The magnetic susceptibility was measured by a SQUID magnetometer (Quantum Design MPMS2).

General methods: UV/Vis absorption spectra were measured on a Hitachi U-3000 absorption spectrometer at room temperature. ^{1}H NMR spectra were measured with a JEOL λ-300 (300 MHz) spectrometer with Me_4Si as internal standard.

Materials: 2,3-Bis(hydroxyamino)-2,3-dimethylbutane was prepared according to the literature method.[26] Other reagents were used as purchased. Column chromatography was performed on silica gel (Merck Silica-gel 60) or alumina (Merck Aluminium Oxide 60). Melting points were recorded on an As one ATM-01 micro melting-point apparatus The stable radical **1** was synthesized according to the procedure shown in Scheme 1.

9-(3-Formylphenyl)anthracene (2): A mixture of 9-bromoanthracene (4.45 g, 17.3 mmol), 3-formylphenylboronic acid (3.0 g, 20 mmol), [Pd-(PPh_3)$_4$] (0.60 g, 0.52 mmol), and K_2CO_3 (9.66 g, 70 mmol) in toluene (120)/EtOH (20)/H_2O (40 mL) was refluxed for 24 h under nitrogen. The organic layer was extracted with toluene, washed with brine, and dried with $MgSO_4$. Evaporation, column chromatography (silica gel, toluene), and crystallization (EtOH) gave **2** in 90% yield (4.41 g, 15.6 mmol) as slightly yellow prisms with m.p. 122 °C: ^{1}H NMR ($CDCl_3$): δ = 7.35–7.37 (m, 2H; ArH), 7.48 (t, J = 7.1 Hz, 2H, ArH), 7.56 (d, J = 8.8 Hz, 2H; ArH), 7.70–7.78 (m, 2H; ArH), 7.96 (s, 1H; ArH), 8.06–8.09 (m, 3H; ArH), 8.54 (s, 1H; ArH), 10.12 ppm (s, 1H; CHO); elemental analysis (%) calcd for $C_{21}H_{14}O$: C 89.34, H 5.00; found: C 89.06, H 4.97.

9-(3-Formylphenyl)-10-bromoanthracene (3): A mixture of **2** (4.40 g, 15.6 mmol) and *N*-bromosuccinimide (NBS, 2.83 g, 16 mmol) in anhydrous DMF (80 mL) was refluxed for 24 h under nitrogen. H_2O (300 mL) was added to the solution. The organic layer was extracted with toluene, washed with brine, and dried ($MgSO_4$). Evaporation and crystallization (toluene) gave **3** in 97% yield (5.45 g, 15.1 mmol) as yellow powder: ^{1}H NMR ($CDCl_3$): δ = 7.39 (t, J = 9 Hz, 2H; ArH), 7.54 (d, J = 8.8 Hz, 2H; ArH), 7.61 (t, J = 6.9 Hz, 2H; ArH), 7.68 (d, J = 7.6 Hz, 1H; ArH), 7.77 (t, J = 7.6 Hz, 1H; ArH), 7.93 (s, 1H; ArH), 8.09 (d, J = 7.6 Hz, 1H; ArH), 8.63 (d, J = 7.9 Hz, 2H; ArH), 10.12 ppm (s, 1H; CHO); elemental analysis (%) calcd for $C_{21}H_{13}BrO$: C 69.82, H 3.63; found: C 70.00, H 3.62.

9-(3-Formylphenyl)-10-(4-formylphenyl)anthracene (4): A mixture of **3** (5.45 g, 15.1 mmol), 4-formylphenylboronic acid (3.0 g, 20 mmol), [Pd-(PPh_3)$_4$] (0.52 g, 0.45 mmol), and K_2CO_3 (8.28 g, 60 mmol) in toluene (100)/EtOH (20)/H_2O (50 mL) was refluxed for 24 h under nitrogen. The organic layer was extracted with toluene, washed with brine, and dried with $MgSO_4$. Evaporation, column chromatography (silica gel, benzene), and crystallization (EtOH/toluene 9/1) gave **4** in 64% yield (3.76 g, 9.7 mmol) as slightly yellow prisms with m.p. 239–240 °C: ^{1}H NMR ($CDCl_3$): δ = 7.35–7.39 (m, 4H; ArH), 7.59–7.81 (m, 8H; ArH), 8.01 (s, 1H; ArH), 8.09–8.16 (m, 3H; ArH), 10.15 (s, 1H; CHO), 10.22 ppm (s, 1H; CHO); elemental analysis (%) calcd for $C_{28}H_{18}O_2$: C 87.02, H 4.69; found: C 87.04, H 4.55.

9-[3-(4,4,5,5-Tetramethyl-1,3-dihydroxyimidazolidin-2-yl)phenyl]-10-[4-(4,4,5,5-tetramethyl-1,3-dihydroxyimidazolidin-2-yl)phenyl]anthracene (5): A mixture of **4** (0.82 g, 2.1 mmol), 2,3-bis(hydroxyamino)-2,3-dimethylbutane (1.25 g, 8.4 mmol), and 2,3-bis(hydroxyamino)-2,3-dimethylbutane monosulfate salt (0.13 g, 0.53 mmol) in MeOH (30)/$CHCl_3$ (30 mL) was stirred for 72 h. After evaporation under reduced pressure, MeOH (5 mL) was added, and then H_2O (20 mL) was added to the resulting homogeneous solution. The deposited powder was collected by filtration, washed with H_2O (20 mL) and MeOH (10 mL), and dried in vacuo to give **5** as a white powder in 65% yield (0.88 g, 1.36 mmol).

9-[3-(4,4,5,5-Tetramethyl-1-yl-oxyimidazolin-2-yl)phenyl]-10-[4-(4,4,5,5-tetramethyl-1-yl-oxyimidazolin-2-yl)phenyl]anthracene (1): A solution of $NaIO_4$ (0.25 g, 1.14 mmol) in H_2O (40 mL) was added to a suspension of of **5** (0.25 g, 0.38 mmol) in toluene (40 mL) and the mixture was stirred for 2 h. The organic layer (dark blue) was separated, washed with brine, dried ($MgSO_4$), and evaporated. After addition of CH_2Cl_2 (20 mL) and $NaNO_2$ (0.26 g, 3.8 mmol) in H_2O (20 mL) to the residue, 1 N HCl was added dropwise to the mixture at 0 °C until the organic layer turned orange.[27] The organic layer was then separated, washed with brine, dried ($MgSO_4$), and evaporated. Column chromatography (alumina, toluene) and recrystallization from EtOH gave **1** in 6.5% yield (0.015 g, 0.025 mmol) as red prisms with m.p. 240–242 °C. Elemental analysis (%) calcd for $C_{40}H_{40}N_2O_2$: C 78.92, H 6.62, N 9.20; found: C 78.76, H 6.71, N 9.01.

A small amount of a monoradical impurity, which was detected by ESR spectroscopy, contaminated the product obtained by the above procedures. Therefore, the product **1** was further purified by column chromatography (alumina, benzene), followed by evaporation of solvent by a freeze-dry method. The purity and biradical concentration were tested by ESR and SQUID measurements. The biradical concentration was confirmed to be higher than 99%. The monoradical contaminant was not detected within the sensitivity of our ESR apparatus after purification.

Acknowledgements

This work was supported by the Grant-in-Aid for Scientific Research on the general (No. 13440211, 16350079) and Priority Area "Application of Molecular Spin" (Area 769, Prop. No. 15087208) from the Ministry of Education, Culture, Sports, Science and Technology, Japan. We also acknowledge Prof. Y. Miura (OCU) for his assistance in the purification of the sample.

[1] Y. Teki, S. Miyamoto, K. Iimura, M. Nakatsuji, Y. Miura, *J. Am. Chem. Soc.* **2000**, *122*, 984.

[2] Y. Teki, S. Miyamoto, M. Nakatsuji, Y. Miura, *J. Am. Chem. Soc.* **2001**, *123*, 294.
[3] Y. Teki, *Polyhedron* **2001**, *20*, 1163.
[4] K. Itoh, *Pure Appl. Chem.* **1978**, *50*, 1251.
[5] Y. Teki and K. Itoh, "Design and Experimental Investigation of High-Spin Organic Systems" in *Magnetic Properties of Organic Materials* (Ed.: P. M. Lahti), Marcel-Dekker, **1999**, pp. 237–265, and references therein.
[6] H. Iwamura, N. Koga, *Acc. Chem. Res.* **1993**, *26*, 346.
[7] T. Sugawara, *Mol. Cryst. Liq. Cryst.* **1999**, *334*, 257.
[8] Recent reviews on molecule-based magnetism: Proceedings of the VIIIth International Conference on Molecule-Based Magnets: *Polyhedron* **2003**, *22*, 1727–2572.
[9] Y. Teki, M. Nakatsuji, Y. Miura, *Mol. Phys.* **2002**, *100*, 1385.
[10] Y. Teki, M. Nakatsuji, Y. Miura, *Int. J. Mod. Phys. B* **2001**, *15*, 4029.
[11] Y. Teki, M. Kimura, S. Narimatsu, K. Ohara, K. Mukai, *Bull. Chem. Soc. Jpn.* **2004**, *77*, 95.
[12] Y. Teki, S. Nakajima, *Chem. Lett.* **2004**, *33*, 1500.
[13] a) A. Izuoka, M. Hiraishi, T. Abe, T. Sugawara, K. Sato, T. Takui, *J. Am. Chem. Soc.* **2000**, *122*, 3234; b) S. Hiraoka, T. Okamoto, M. Kozaki, D. Shiomi, K. Sato, T. Takui, K. Okada, *J. Am. Chem. Soc.* **2004**, *126*, 58.
[14] a) K. Matsuda, M. Matsuo, M. Irie, *Chem. Lett.* **2001**, *5*, 436; b) K. Matsuda, M. Irie, *J. Am. Chem. Soc.* **2001**, *123*, 9896; c) K. Takayama, K. Matsuda, M. Irie, *Chem. Eur. J.* **2003**, *9*, 5605.
[15] a) C. Corvaja, M. Maggini, M. Prato, G. Scorrano, M. Venzin, *J. Am. Chem. Soc.* **1995**, *117*, 8857; b) N. Mizouchi, Y. Ohba, S. Yamauchi, *J. Chem. Phys.* **1997**, *101*, 5966; c) P. Ceroni, F. Conti, C. Corvaja, M. Maggini, F. Paolucci, S. Roffia, G. Scorrano, A. Toffoletti, *J. Phys. Chem. A* **2000**, *104*, 156; d) N. Mizouchi, Y. Ohba, S. Yamauchi, *J. Phys. Chem. A* **1999**, *103*, 7749; e) F. Conti, C. Corvaja, A. Toffoletti, N. Mizouchi, C. Y. Ohba, S. Yamauchi, M. Maggini, *J. Phys. Chem. A* **2000**, *104*, 4962; f) J. Fujiwara, Y. Iwasaki, Y. Ohba, S. Yamauchi, N. Koga, S. Karasawa, M. Fuhs, K. Möbius, S. Weber, *Appl. Magn. Reson.* **2001**, *21*, 483.
[16] a) K. Ishii, J. Fujiwara, Y. Ohba, S. Yamauchi, *J. Am. Chem. Soc.* **1996**, *118*, 13079; b) K. Ishii, J. Fujisawa, A. Adachi, S. Yamauchi, N. Kobayashi, *J. Am. Chem. Soc.* **1998**, *120*, 3152; c) K. Ishii, Y. Hirose, N. Kobayashi, *J. Phys. Chem. A* **1999**, *103*, 1986.
[17] a) T. Immamura, O. Onitsuka, K. Obi, *J. Phys. Chem.* **1986**, *90*, 167; b) C. Blätter, J. F. Paul, *Chem. Phys. Lett.* **1990**, *166*, 375; c) Y. Kobori, M. Mitsui, A. Kawai, K. Obi, *Chem. Phys. Lett.* **1996**, *252*, 355, and references therein.
[18] W. T. Borden, E. R. Davidson, *J. Am. Chem. Soc.* **1976**, *98*, 4587.
[19] G. G. Belford, R. L. Belford, J. F. Burkhalter, *J. Magn. Reson.* **1973**, *11*, 251.
[20] Y. Teki, I. Fujita, T. Takui, T. Kinoshita, K. Itoh, *J. Am. Chem. Soc.* **1994**, *116*, 11499. In the spectral simulation of the TRESR spectra, the calculation of ESP has been added as a subroutine to the computer program. The details of the spectral simulation for high-spin organic molecules are similar to those described in our previous paper on the perturbation approach: Y. Teki, T. Takui, H. Yagi, K. Itoh, H. Iwamura, *J. Chem. Phys.* **1985**, *83*, 539.
[21] a) J. Isoya, H. Kanda, J. R. Norris, J. Tang, M. K. Bowman, *Phys. Rev. B* **1990**, *41*, 3905; b) A. V. Astashkin, A. Schweiger, *Chem. Phys. Lett.* **1990**, *174*, 595.
[22] K. Sato, M. Yano, M. Furuichi, D. Shiomi, T. Takui, K. Abe, K. Itoh, A. Higuchi, K. Katsuma, Y. Shirota, *J. Am. Chem. Soc.* **1997**, *119*, 6607.
[23] The g, D, and E values of the T1 state of anthracene in an EPA rigid matrix were determined to be $g=2.003$, $D=0.0710\ \mathrm{cm}^{-1}$, and $E=0.0070\ \mathrm{cm}^{-1}$.
[24] See Figure 14 in reference [2] or Figure 7 in reference [3].
[25] A triplet state between a photoexcited singlet and a quintet state was preliminary reported for a fullerene bis(nitroxide) (Y. Ohba, M. Nishimura, N. Mizouchi, S. Yamauchi, *Appl. Magn. Reson.* **2004**, *26*, 117). However, the D value is close to that of the triplet state of the fullerene derivative. The counterpart of another triplet state was tentatively assigned as the broad signal in the center of the spectrum. The triplet state with a reduced D value was not clearly assigned. The transient nutation phenomena were not observed.
[26] a) M. Lamchen, T. W. Mittag, *J. Chem. Soc. C* **1966**, *2*, 300; b) C. Hirel, K. E. Vostrikova, J. Pecaut, V. I. Ovcharenko, P. Rey, *Chem. Eur. J.* **2001**, *7*, 2007.
[27] a) E. F. Ullman, L. Call, J. H. Osiecki, *J. Org. Chem.* **1970**, *35*, 3623; b) E. F. Ullman, J. H. Osiecki, D. G. B. Boocock, R. Darcy, *J. Am. Chem. Soc.* **1972**, *94*, 7079; c) D. Gatteshi, P. Rey, "Design, Synthesis, and Properties of Nitroxide Networked Material" in *Magnetic Properties of Organic Materials* (Ed.: P. M. Lahti), Marcel-Dekker, **1999**, 601–627.
[28] We have carried out an additional pulsed-ESR experiment using a 1 kW TWTA amplifier instead of the 10 W solid-state amplifier. In this experiment, the condition of $\omega_1 \gg \omega_{ZFS}$ is safely satisfied ($B_1=$ 1.4 mT). The ratio of the nutation frequency was improved to 1.42, which is just the expected value for the triplet state.

Received: August 12, 2005
Published online: December 22, 2005

